Absolute doubly differential single-ionization cross sections in $p+$He collisions

M. Schulz, T. Vajnai,* A. D. Gaus, W. Htwe,† D. H. Madison, and R. E. Olson
Department of Physics and the Laboratory for Atomic and Molecular Research, University of Missouri–Rolla, Rolla, Missouri 65401
(Received 7 February 1996)

We have measured and calculated doubly differential single-ionization cross sections for 50–150-keV $p+$He collisions as a function of the projectile energy loss and scattering angle. The measured cross sections were put on an absolute scale by normalizing the integrated cross sections to known total cross sections. Clear effects of the postcollision interaction (PCI) were observed in the scattered projectile spectra. Our singly differential cross sections as a function of projectile energy loss do not agree with corresponding cross sections obtained from electron spectroscopy. These discrepancies are attributed to the PCI. Our calculations including the PCI reproduce the shape of our data quite well; however, there are discrepancies in the absolute magnitude. [S1050-2947(96)06807-2]

PACS number(s): 34.50.Fa, 34.50.Bw

INTRODUCTION

Ion-atom collisions have been studied for many decades. Nevertheless, even the most fundamental inelastic processes (excitation, capture, and ionization) occurring in the most simple collision systems are not completely understood. From a theoretical point of view, the basic problem is that the Schrödinger equation is not solvable for more than two bodies without using approximations. The major difficulties one encounters are quite different in nature for the three fundamental processes mentioned above. State-selective excitation cross sections, both total and differential in the projectile solid angle, are reproduced reasonably well by various calculations [1,2]. However, not much experimental data is currently available on the magnetic substate population in excitation processes for heavy projectiles. Although such data for electron impact have been available for many years [3], for a long time these data were not reproduced by calculations even qualitatively [4]. It is only very recently that theoretical calculations have been performed which are in accord with experiment [5]. In the case of capture processes, a major theoretical problem arises from the fact that the electron changes its frame of reference during the collision. The correct description of this change of frame of reference is a difficult task, involving the introduction of translational factors [6,7]. Ionization is perhaps the most difficult process to treat theoretically. One major problem is the description of the continuum state of the ionized electron. Because of the long-range nature of the Coulomb force it is critical to properly represent the asymptotic behavior of these continuum states by three-body Coulomb wave functions [8,9]. Furthermore, reaction channels other than ionization can be coupled to the continuum. This can lead to complex interference effects in the ionized electron spectra [10].

Because of the problems related to the long-range nature of the Coulomb force, it is clear that in perturbation theory it is not sufficient to treat ionization using a first-order calculation. Madison [11] has shown that treating the target ion-electron interaction to all orders leads to a much better description of measured electron spectra for ionizing collisions than first-order calculations. However, it is also well known that the projectile-electron interaction must be treated beyond first order as well. In the pioneering experiments of Crooks and Rudd [12] and Harrison and Lucas [13] for proton impact ionization, pronounced, cusp-shaped peaks were found in the ionized electron spectra at electron energies corresponding to the projectile velocity for emission angles near 0°. It was shown that these cusp electrons owe their existence to the fact that the electrons experience the projectile field even after traveling a long distance from the collision region. Due to this projectile-electron interaction after the projectile-target collision [postcollision interaction (PCI)] the ionized electron is focused toward the projectile, which leads to the cusp peak at an electron energy corresponding to the projectile velocity. Therefore, the PCI, which is not taken into account by first-order calculations, has to be properly treated by theories on electron emission in the forward direction [14,15].

Since the initial discovery of cusp electrons, the importance of the PCI in ionizing collisions was established in a large number of experiments [16–25] and theoretical studies [26–29]. One conclusion that was drawn from these studies was that even though cusp electrons are important for emission angles near 0°, their contribution to the cross sections integrated over all electron angles was insignificant. Olson *et al.* [28] and Gay *et al.* [19] reported indications that the PCI can also lead to an enhancement of electrons traveling on the saddle of the potential between the projectile and the target nucleus. Recently, we have reported evidence that the much heavier projectile can also be significantly affected by the PCI [25]. Clear effects of the PCI were observed in the doubly differential ionization cross sections as a function of the projectile scattering angle and the ionized electron energy. Furthermore, it was concluded that the contributions from cusp electrons to these doubly differential cross sections are not negligible, even though they are integrated over all electron angles. Similar effects were also seen in our calculations which included the PCI. That work was focused on

*Present address: Department of Physics, University of Miskolc, Miskolc, H-3515, Hungary.
†Present address: Division of Arts and Sciences, Spoon River College, RR1, Canton, IL 61520.

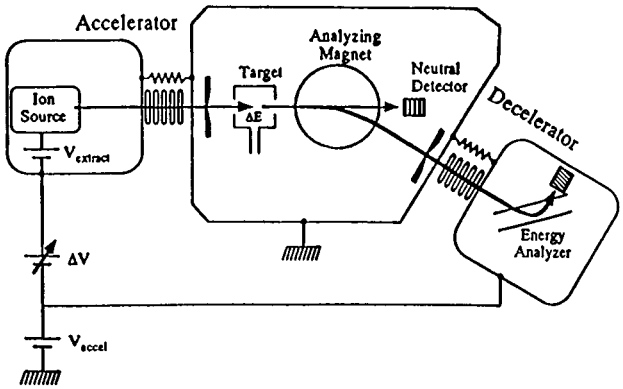

FIG. 1. Schematics of the ion energy-loss spectrometer.

the shape of the doubly differential cross sections as a function of scattering angle and the electron energy. In this paper we present absolute magnitudes of both the doubly differential cross sections and singly differential (integrated over scattering angle) cross sections. We show that even in these singly differential cross sections as a function of electron energy there is an observable effect of the PCI between the projectile and the ionized electron leading to cusp electrons. We compare our data to singly differential cross sections obtained by electron spectroscopy [30,31]. In these latter studies, electrons were only measured for emission angles of 10° and larger. Since cusp electrons are strongly forward peaked, they were thus heavily suppressed in these measurements.

EXPERIMENT

The experiment was performed on the ion energy-loss spectrometer (IELS) at the University of Missouri—Rolla. The schematic of the apparatus is shown in Fig. 1. A proton beam with a very narrow energy spread ($\ll$1 eV) was produced in a hot cathode ion source and extracted at an energy of 2 keV. The beam was then accelerated to energies of 50, 75, 100, and 150 keV and steered through a differentially pumped target gas cell. A set of slits right in front of the gas cell was used to collimate the beam to a size of 0.1 mm$\times$0.1 mm. The projectile charge states after the collision were separated with a switching magnet. The protons then passed through a solid-angle defining collimator and were decelerated to an energy of 2 keV. The projectiles were energy analyzed using a 45° parallel plate analyzer [32] and detected by a discrete dynode electron multiplier.

The energy analyzer was set to a fixed pass energy of 2 keV. Projectile energy-loss spectra were taken by scanning an offset voltage ΔV on the accelerator relative to the decelerator. After acceleration, but before the collision region, the protons therefore had an energy of 2 keV$+(V_{\rm dec}+\Delta V)q$, where $V_{\rm dec}$ is the decelerator potential and 2 keV comes from the ion source extraction. After the collision and after deceleration the energy was 2 keV$+\Delta V-\epsilon$, where ϵ is the energy loss the projectiles suffered in the collision. When the energy loss was equal to the offset voltage, the protons entered the energy analyzer with the pass energy and were detected. The projectile scattering angle was scanned by pivoting the accelerator about the center of the target chamber.

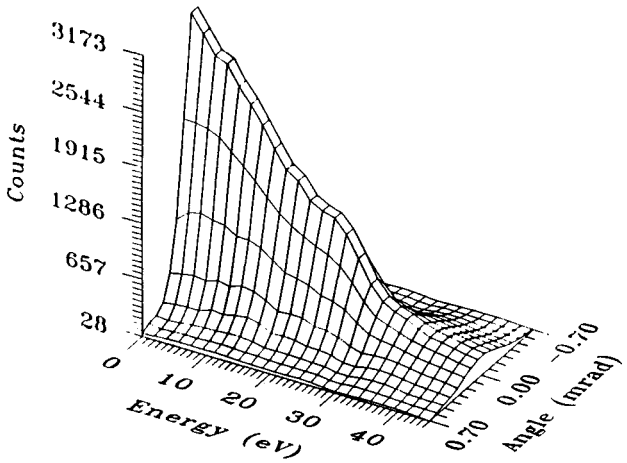

FIG. 2. Measured doubly differential ionization cross sections for 50-keV $p+$He collisions as a function of the projectile scattering angle and the ionized electron energy.

For each projectile energy, the measurements consisted of three parts. First, an angular scan of the incident beam (zero energy loss) with no target gas was taken. From the angular distribution of the incident beam, we found an overall angular resolution of ± 75 μrad. Second, an energy-loss spectrum was taken for the target gas covering a range from -5 eV to either 80 or 150 eV (depending on projectile energy) for a fixed scattering angle of 0°. The width of the peak representing the incident beam (zero energy loss) indicates an overall energy resolution of 1.5 eV full width at half maximum (FWHM). These energy-loss spectra enabled us to determine relative doubly differential ionization cross sections at 0° as a function of the energy loss. Finally, the angular distribution of protons with fixed energy loss was measured. These measurements were then repeated for energy losses ranging from 26 eV to either 80 or 150 eV (depending on projectile energy). The angular distribution of the incident beam (zero energy loss) from the first measurement was used to deconvolute the incident beam divergence [33] from the measured angular distributions of the ionizing protons obtained in the third measurements. From this procedure we obtained relative doubly differential ionization cross sections at fixed energy losses as a function of scattering angle. From the combination of the second and third measurements, we thus obtained relative doubly differential ionization cross sections as a function of both scattering angle and projectile energy loss. The cross sections were put on an absolute scale by normalizing the cross sections integrated over both scattering angle and energy loss to accurately known total ionization cross sections [34]. A target pressure dependence was taken to ensure single collision conditions. The experiment was performed with a target pressure of 50 mTorr over a length of about 1 cm.

RESULTS AND DISCUSSION

In Fig. 2 we show a three-dimensional plot of the relative doubly differential cross sections as a function of the projectile scattering angle and the ionized electron energy for a projectile energy of 50 keV. The electron energy is given by the projectile energy loss minus the ionization potential.

TABLE I. Measured doubly differential ionization cross sections as a function of the projectile scattering angle and the ionized electron energy for 50-keV p+He collisions.

	$d^2\sigma/d\Omega\ dE$ (10^{-13} cm^2/sr eV)											
θ (mrad)	1 eV	5 eV	10 eV	17 eV	22 eV	23 eV	26 eV	27 eV	29 eV	31 eV	40 eV	45 eV
0	115	88	75	54	52	50	40	33	24	19	9.8	7.2
0.04	114	85	71	52	51	51	37	31	24	18	10	7.6
0.06	108	81	69	51	52	47	37	31	24	18	9.6	7.3
0.08	97	80	66	48	45	46	32	28	23	18	9.1	7.1
0.10	91	75	59	45	44	42	30	28	22	18	8.7	6.7
0.15	70	58	48	36	36	34	24	24	19	16	8.5	6.5
0.20	48	43	36	29	29	27	18	20	17	13	7.6	5.9
0.25	32	30	27	21	20	19	15	16	13	11	6.6	5.3
0.30	21	18	19	14	15	14	11	11	10	8.5	5.5	4.4
0.35	12	12	12	10	11	9.6	9.3	8.0	7.9	6.7	4.8	3.7
0.40	8.3	8.0	8.8	7.2	7.8	7.2	6.1	5.7	5.4	5.5	3.7	3.1
0.45	7.4	5.6	7.5	5.6	6.2	5.9	5.4	4.8	4.4	4.2	2.9	2.8
0.50	4.5	4.1	4.5	3.9	4.4	4.2	3.9	3.4	3.6	3.2	2.3	2.4
0.55	3.7	3.3	3.6	3.2	3.7	3.1	2.8	3.0	3.0	2.9	2.1	2.2
0.60	3.4	3.0	3.1	2.9	3.0	3.0	2.5	2.7	2.5	2.7	1.7	1.6
0.65	2.7	2.4	2.3	2.4	2.4	2.1	2.4	2.3	1.9	2.0	1.7	1.2
0.70	2.2	2.7	2.4	2.3	2.3	2.4	2.0	2.3	1.7	1.4	1.7	0.8

These cross sections drop rapidly with increasing scattering angle and ionized electron energy. Furthermore, there is a pronounced shoulder at an electron energy around 25 eV for small scattering angles. This energy approximately corresponds to $E_e = m/ME_p$, where E_e is the electron energy, E_p is the projectile energy, and m/M is the electron-to-projectile-mass ratio. Electrons with this energy move at the same speed as the projectile (matching velocity). For all projectile energies which we measured, a structure was observed around an electron energy corresponding to the matching velocity. In an earlier article [25], we demonstrated that these structures are due to the postcollision interaction between the ionized electron and the outgoing projectile, which is the same mechanism leading to the well-known cusp peak in the electron spectra.

As mentioned above, absolute doubly differential ionization cross sections were obtained by normalizing the relative cross sections integrated over both ionized electron energy and projectile scattering angle to well-known total cross sections [34]. These absolute doubly differential cross sections are listed for all projectile energies in Tables I–IV and they are displayed for a subset of electron energies as the solid circles in Figs. 3–6. In these plots, the cross sections are presented for fixed incident projectile energies and fixed ejected electron energies as a function of the projectile scattering angle. For proton scattering angles larger than about 1 mrad, the count rate of projectiles coming from collisions with the He target gas was not much larger than the background count rate coming from collisions with the residual gas and from dark counts of the detector. Therefore, at these

TABLE II. Same as Table I for 75 keV.

	$d^2\sigma/d\Omega\ dE$ (10^{-13} cm^2/sr eV)												
θ (mrad)	1 eV	5 eV	10 eV	20 eV	25 eV	30 eV	35 eV	38 eV	40 eV	42 eV	45 eV	50 eV	55 eV
0	184	132	92	56	48	42	36	31	23	18	15	11	8.5
0.05	154	138	102	48	42	42	34	37	27	21	15	10	7.7
0.10	117	112	79	44	38	37	29	29	20	17	13	9.6	7.4
0.15	86	85	62	36	31	30	23	24	16	14	12	8.4	7.0
0.20	49	56	46	27	25	23	19	19	13	13	10	7.7	5.5
0.30	22	24	22	13	13	13	12	12	8.6	7.9	6.9	5.1	4.1
0.40	9.6	8.4	10	6.7	6.3	5.5	6.0	6.7	4.5	4.1	4.0	3.2	2.8
0.50	3.5	3.3	4.0	2.6	2.0	2.3	3.4	3.4	3.2	2.5	1.9	2.0	1.7
0.60	2.3	2.1	2.2	1.8	1.0	1.3	1.8	2.1	1.6	1.6	1.2	1.1	0.90
0.70	2.4	1.3	1.5	0.84	0.84	0.91	1.1	1.3	0.69	0.79	0.88	0.55	0.60
0.80	1.2	1.0	0.92	0.57	0.44	0.87	0.58	0.76	0.52	0.48	0.55	0.39	0.51
0.90	0.61	0.60	0.32	0.55	0.67	0.57	0.64	0.47	0.44	0.35	0.63	0.54	0.36
1.00	0.32	0.61	0.40	0.54	0.28	0.45	0.46	0.60	0.41	0.46	0.37	0.26	0.22
1.20	0.21	0.23	0.24	0.37	0.24	0.14	0.25	0.34	0.13	0.12	0.09	0.24	0.23
1.50	0.04	0.21	0.19	0.19	0.09	0.15	0.07	0.03	0.14	0.18	0.09	0.13	0.07

TABLE III. Same as Table I for 100 keV.

	$d^2\sigma/d\Omega\ dE$ (10^{-13} cm^2/sr eV)																	
θ (mrad)	5 eV	10 eV	15 eV	20 eV	25 eV	30 eV	35 eV	40 eV	42 eV	44 eV	45 eV	48 eV	50 eV	53 eV	55 eV	60 eV	65 eV	75 eV
0	138	91	65	56	44	26	31	25	25	44	24	23	23	19	17	12	9.1	7.2
0.05	112	78	50	49	36	35	30	25	29	23	23	21	20	17	14	12	8.8	7.1
0.10	88	62	43	42	30	29	28	22	21	20	19	17	17	14	14	11	8.2	6.0
0.15	61	43	32	32	23	25	24	18	17	16	16	14	15	12	12	9.5	6.9	5.8
0.20	36	27	21	23	16	18	17	15	14	12	13	11	12	10	9.0	8.3	6.0	5.0
0.30	14	13	8.8	11	8.2	9.3	9.0	8.5	8.1	7.4	7.8	6.2	6.8	6.0	5.3	5.1	4.2	3.8
0.40	4.9	5.6	3.6	4.8	4.9	4.4	4.6	3.7	3.8	4.2	3.3	3.3	3.1	3.3	3.3	3.2	2.4	2.5
0.50	2.0	2.1	1.1	2.2	1.7	1.6	1.9	1.9	2.2	1.9	1.6	1.6	1.3	1.7	1.8	1.3	1.4	1.4
0.60	1.7	1.6	0.79	1.3	1.1	1.0	0.96	0.63	1.2	1.0	0.97	1.1	0.78	1.1	1.0	0.74	0.84	0.85
0.70	0.69	0.96	0.53	0.69	0.98	0.38	0.49	0.40	0.56	0.51	0.44	0.50	0.52	0.60	0.62	0.47	0.45	0.50
0.80	0.56	0.57	0.27	0.46	0.36	0.63	0.44	0.38	0.44	0.57	0.38	0.51	0.43	0.40	0.40	0.26	0.27	0.30
0.90	0.37	0.51	0.33	0.28	0.25	0.37	0.43	0.38	0.18	0.14	0.25	0.19	0.24	0.31	0.30	0.21	0.22	0.27
1.00	0.15	0.19	0.04	0.25	0.18	0.22	0.20	0.35	0.19	0.21	0.20	0.23	0.14	0.15	0.37	0.16	0.17	0.17
1.20	0.07	0.05	0.04	0.03	0.07	0.11	0.07	0.15	0.13	0.11	0.46	0.06	0.09	0.66	0.18	0.12	0.13	0.09
1.50	0.01	0.02	0.04	0.06	0.03	0.11	0.03	0.08	0.02	0.07	0.09	0.07	0.06	0.08	0.08	0.06	0.05	0.04

large scattering angles, the experimental uncertainties are quite large. At scattering angles smaller than 1 mrad, in contrast, the statistical errors are negligible. Here, the experimental uncertainties are mainly due to the deconvolution of the incident beam profile and due to the normalization procedure. The deconvolution affects scattering angles near 0° particularly sensitively so that here the uncertainties are larger than at intermediate angles, in spite of the larger count rate at small scattering angles.

In Figs. 3–6 we also compare the experimental data to our calculations. The dashed curve shows a distorted-wave Born calculation [11] which treats the target ion-electron interaction to all orders. The projectile-electron interaction, in contrast, is only included in first order so that the PCI is taken into account only very weakly. Furthermore, the target nucleus-projectile interaction is not included either, so that the projectiles are only deflected by their interaction with the electron. Nevertheless, this calculation has been demonstrated to reproduce ionized electron spectra for $p+$He collisions at projectile energies as low as 50 keV reasonably well [11,35]. The full curve represents the same type of Born calculation as the dashed curve; however, here the PCI is incorporated following the method of Salin [15]. In this method the PCI is included by multiplying the transition amplitudes by a Coulomb factor which is proportional to $(v_e - v_p)^{-1}$, where v_e and v_p are the electron and projectile velocities. For convenience, we call the Born calculation without PCI $B1$ and the one with PCI $B2$. The open circles in Figs. 3, 5, and 6 show our classical trajectory Monte Carlo calculations (CTMC). This calculation includes the PCI as well as the interaction between the projectile and the target nucleus.

TABLE IV. Same as Table I for 150 keV.

	$d^2\sigma/d\Omega\ dE$ (10^{-13} cm^2/sr eV)												
θ (mrad)	5 eV	15 eV	25 eV	35 eV	45 eV	55 eV	65 eV	75 eV	77 eV	79 eV	81 eV	83 eV	85 eV	95 eV
0	153	71	46	32	22	16	12	9.9	9.5	8.6	7.6	6.6	5.6	4.2
0.05	132	61	41	29	21	13	12	9.7	8.8	8.1	8.2	6.8	6.3	4.2
0.10	98	43	32	23	18	12	11	9.1	7.6	7.7	7.1	5.7	5.4	3.7
0.15	65	31	25	17	16	9.7	9.2	7.2	7.2	6.8	6.1	5.3	4.7	3.3
0.20	30	16	15	12	12	7.5	7.1	6.5	5.8	5.3	4.9	4.5	4.0	3.0
0.30	9.8	6.9	6.5	7.6	6.6	4.1	4.4	3.8	3.7	3.6	3.3	2.5	2.7	1.9
0.40	2.5	3.0	2.8	3.3	2.8	2.2	2.0	2.2	1.9	2.1	1.6	1.4	1.5	1.2
0.50	0.66	0.99	0.70	1.1	1.2	0.90	0.92	1.1	1.0	0.96	0.81	1.1	0.93	0.73
0.60	0.46	0.42	0.44	0.84	0.85	0.61	0.40	0.67	0.64	0.61	0.77	0.43	0.66	0.61
0.70	0.65	0.17	0.24	0.52	0.35	0.39	0.13	0.45	0.50	0.40	0.94	0.23	0.39	0.31
0.80	0.42	0.13	0.19	0.43	0.44	0.30	0.19	0.30	0.24	0.41	0.40	0.16	0.29	0.24
0.90	0.30	0.17	0.19	0.33	0.28	0.28	0.26	0.32	0.24	0.18	0.26	0.18	0.24	0.21
1.00	0.33	0.27	0.14	0.20	0.33	0.32	0.17	0.35	0.10	0.15	0.24	0.22	0.22	0.25
1.20	0.24	0.06	0.03	0.18	0.18	0.12	0.14	0.20	0.16	0.47	0.20	0.16	0.17	0.23
1.50	0.12	0.14	0.11	0.10	0.14	0.13	0.29	0.23	0.18	0.18	0.20	0.29	0.14	0.20

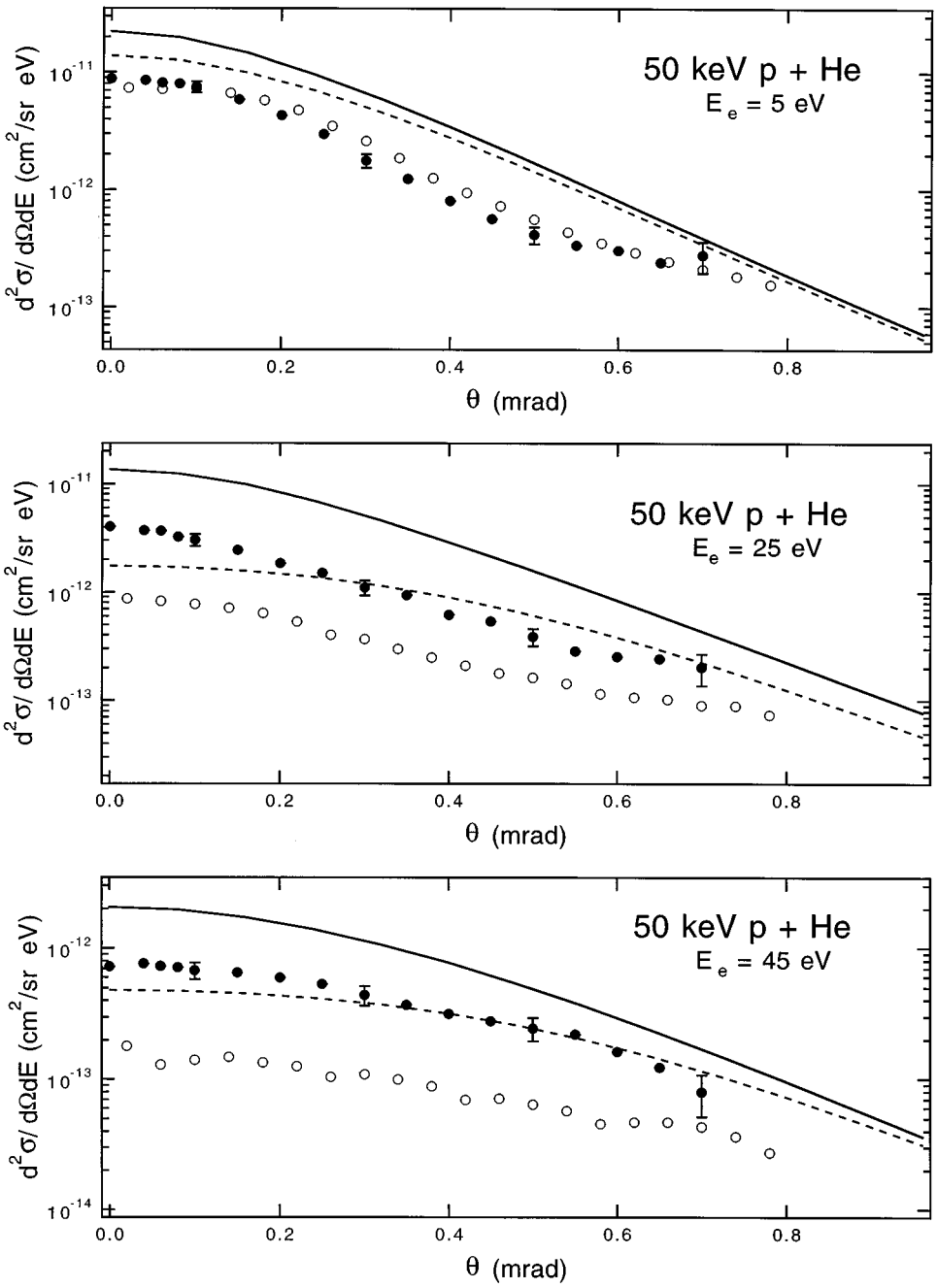

FIG. 3. Doubly differential ionization cross sections as a function of the projectile scattering angle for a subset of fixed electron energies for 50-keV p+He collisions. The solid points are the experimental data, the dashed curve shows our Born calculation without PCI, the solid curve our Born calculation with PCI, and the open circles represent the CTMC calculation.

At a projectile energy of 50 keV and for small electron energies, the CTMC calculation is in nearly perfect agreement with the data. Both Born calculations describe the shape of the measured cross sections well, but they somewhat overestimate the magnitude for small electron energies. At an electron energy of 25 eV, which is the energy where the cusp peak occurs in the electron spectra at this projectile energy, the shape of the $B1$ calculation is significantly different from the shape of the experimental data. Both calculations including the PCI (CTMC and $B2$), on the other hand, describe the shape quite well, even though the agreement is not very good in the absolute magnitude. The CTMC calculation shows increasing discrepancies in the absolute magnitude to the data with increasing electron energy. A similar comparison between the theories and the data is observed for electron energies above the cusp energy. However, with increasing electron energy, the difference between the two Born calculations decreases systematically.

With increasing projectile energy, the agreement of the $B2$ and the CTMC calculations with the experimental data becomes increasingly better. At 150 keV the agreement of both calculations with the data is quite good both in magnitude and shape. The $B1$ calculation, in contrast, still shows significant discrepancies except for small electron energies. The CTMC calculation tends to exhibit better agreement with the data for large scattering angles than the $B2$ calculation. This can be understood by the fact that the $B2$ calculation does not include the projectile-target nucleus interaction. Therefore, in the Born calculation the projectile can only be deflected from the target electron. For a proton scattering from a free electron at rest, there is a classical maximum scattering angle of 0.55 mrad. The contributions in the

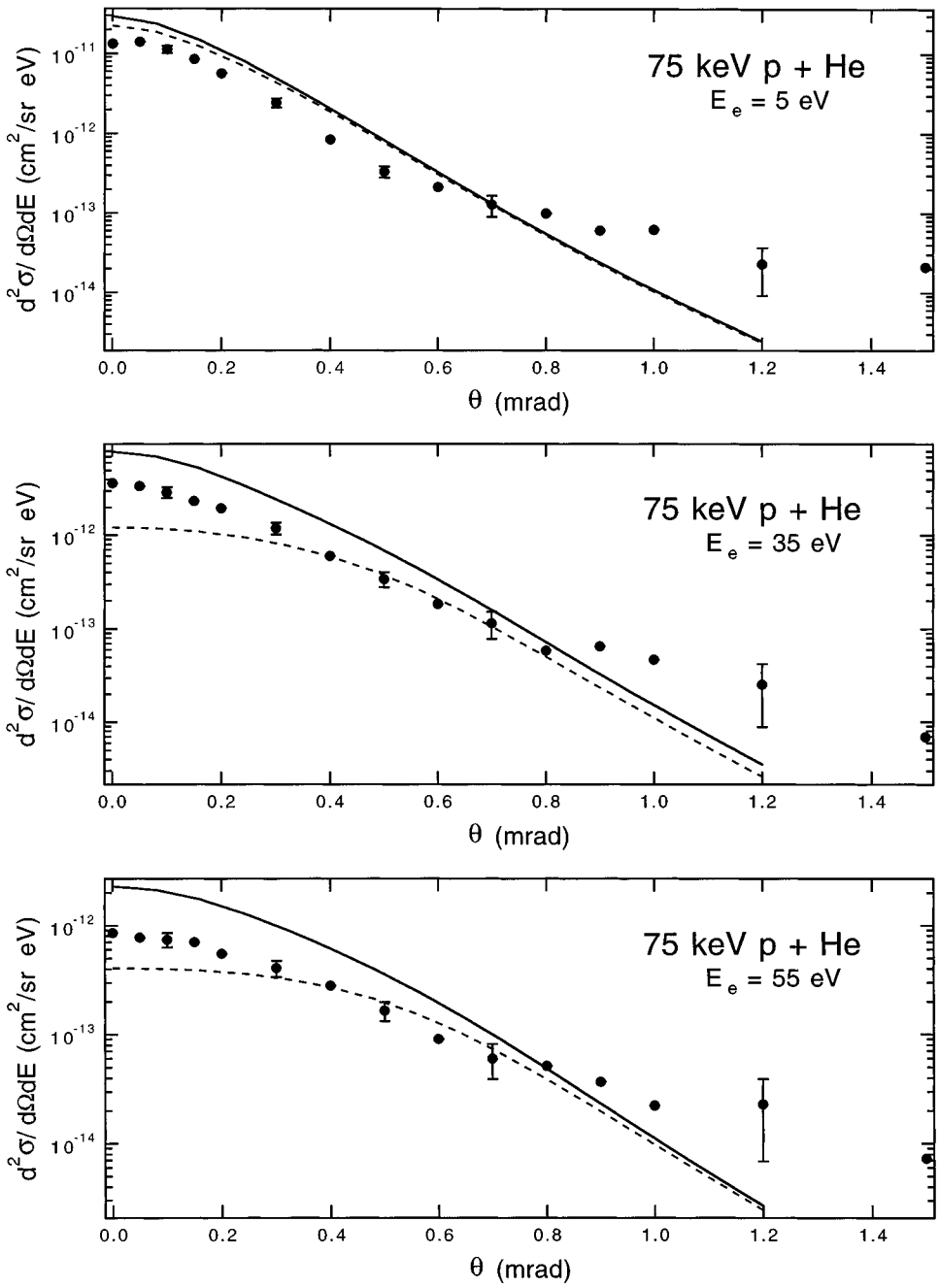

FIG. 4. Same as Fig. 3 but for 75 keV.

$B2$ calculation above this angle are primarily due to the momentum distribution of the electron in the initial target state. Nevertheless, due to the missing projectile-target nucleus interaction, the contributions at large scattering angles are strongly underestimated.

The better overall agreement of the $B2$ and CTMC calculations with the data compared to the $B1$ calculation suggests that the doubly differential cross sections are significantly affected by the PCI. In particular, the shape of the measured cross sections is much better reproduced by the calculations including the PCI. This is illustrated in Fig. 7, where the half widths at half maximum of the angular distributions of the doubly differential cross sections for fixed electron energies are plotted as a function of electron velocity relative to the projectile velocity. The symbols and curves have the same meaning as in Figs. 3–6. In the case of the experimental data, the widths were obtained from a fit of a combination of a Gaussian and a Lorentzian function to the data. The measured widths show the expected general trend, i.e., they increase with increasing electron velocity. However, contrary to our expectation, at the matching velocity ($v_e/v_p=1$), which corresponds to the cusp energy, a distinct change of the slope is observed. Below the matching velocity, the width increases relatively slowly while it increases much more steeply above the matching velocity. This effect appears to become weaker with increasing projectile energy and it is not observed at 150 keV. Qualitatively, the CTMC and $B2$ calculations show similar features. Both calculations also show a change of slope and in some cases even a minimum is observed near the matching velocity. At the low projectile energies, there appears to be some indication for such minima in the experimental data as well; however, at

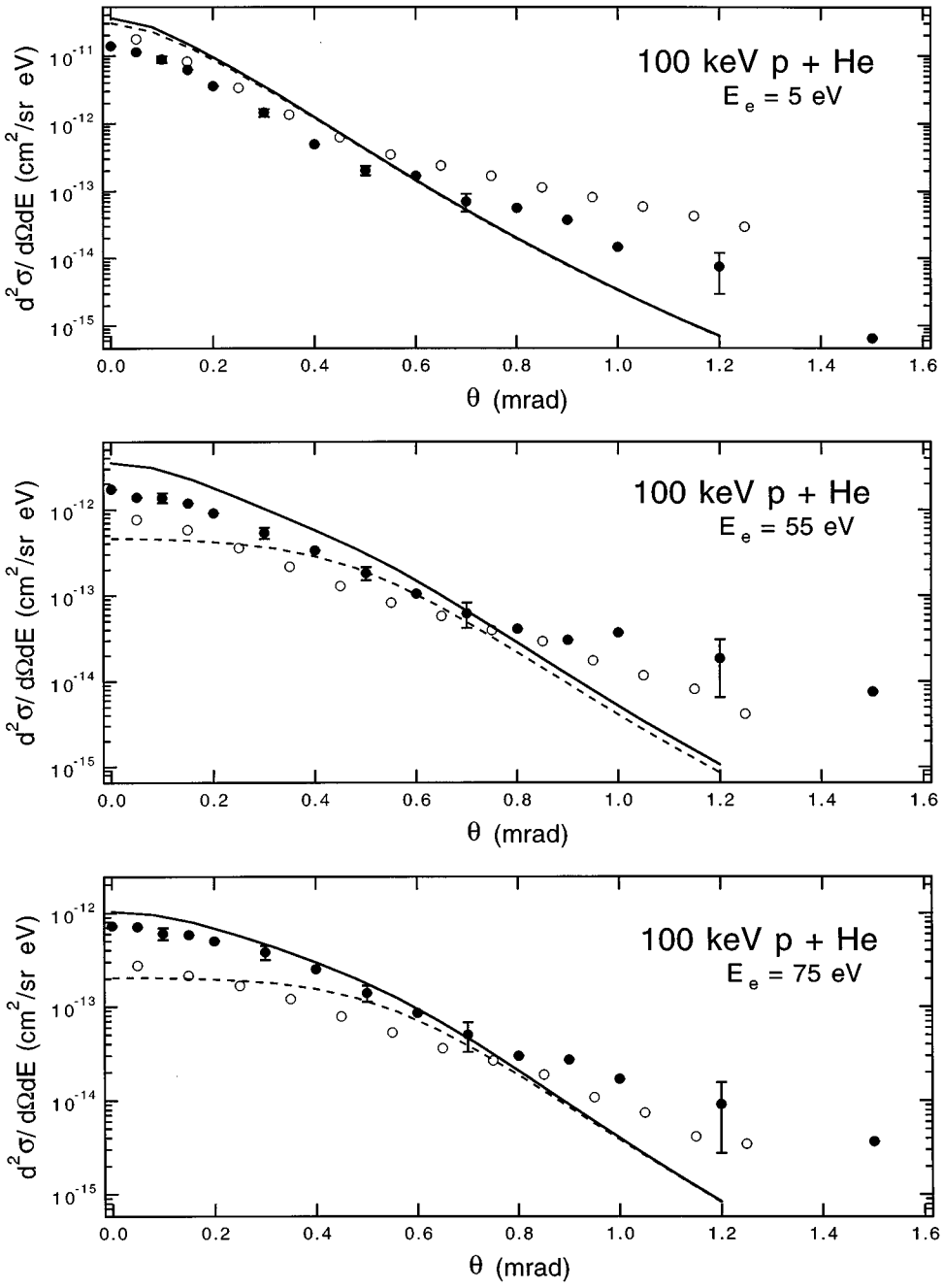

FIG. 5. Same as Fig. 3 but for 100 keV.

the higher projectile energies there are certainly no minima as pronounced as in the $B2$ calculation. Otherwise, these calculations are in fair agreement with the data. The $B1$ calculation, in contrast, drastically overestimates the widths with the largest discrepancies occurring at the matching velocity. In a recent paper, we have interpreted these observations as due to the postcollision interaction [25].

In the electron spectra obtained directly from electron spectroscopy, the cusp electrons are only observed at electron emission angles around 0°. It was therefore assumed that the PCI has a significant effect only on cross sections doubly differential in the electron energy and the electron ejection angle, and it was thought to be negligible in the cross sections integrated over all electron angles. In our experiment, the cross sections are automatically integrated over all electron angles. Our results thus appear to call the above assumptions into question. On the other hand, it should be noted that our cross sections are differential in the projectile angle. Furthermore, it cannot be ruled out that the projectile angle is correlated with the electron angle such that if one selects small projectile scattering angles, small electron emission angles are favored as well. In that case the importance of the PCI in our doubly differential cross sections would be less surprising at least for the small scattering angles, where indeed the effect of the PCI appears to be most pronounced (see Fig. 2). It is therefore important to also analyze the singly differential cross sections integrated over all projectile angles.

In Figs. 8–11 we show the ionization cross sections singly differential in the ionized electron energy as a function of the ratio of the electron velocity to the projectile velocity (relative electron velocity). The data show similar features as the

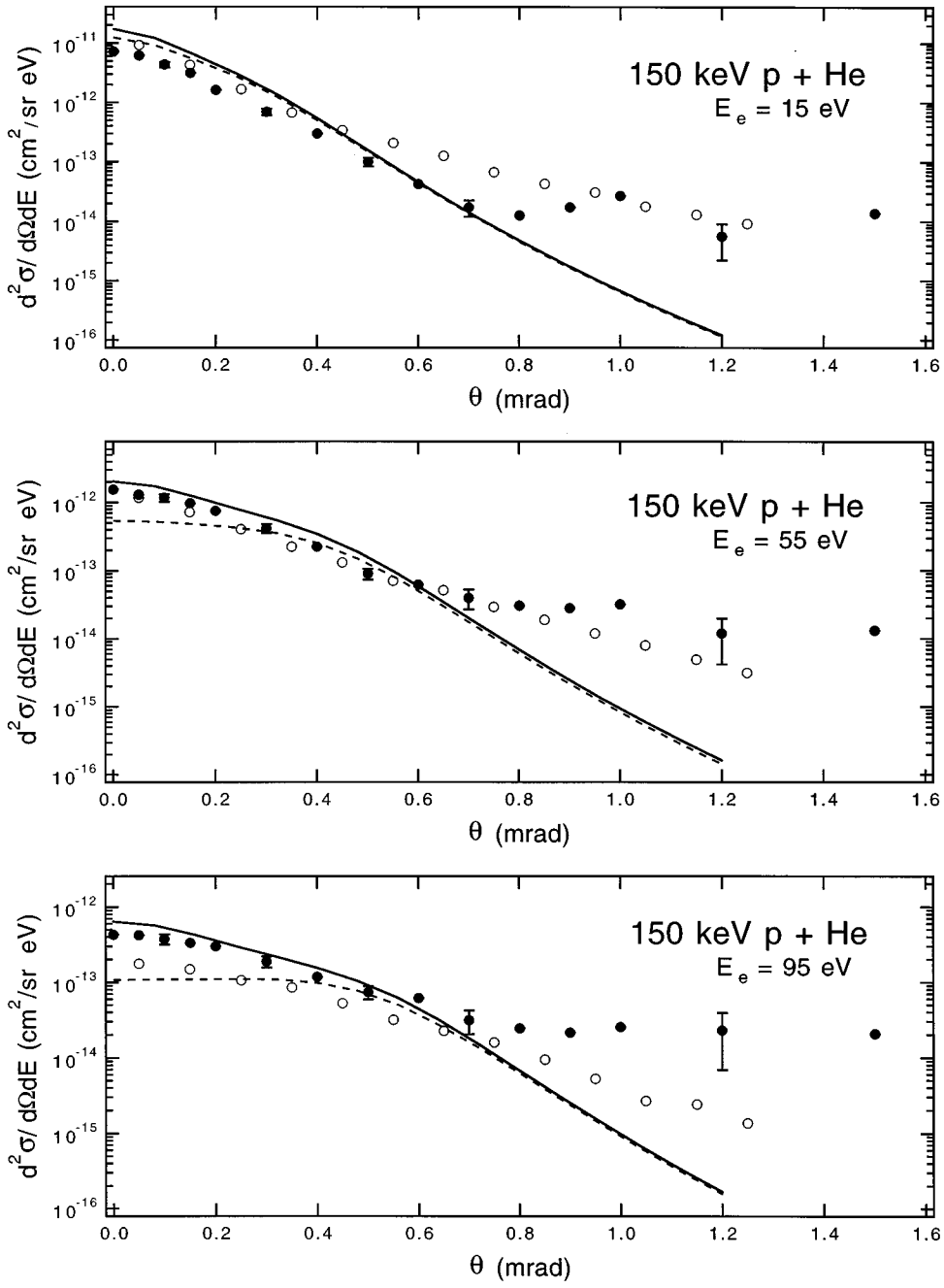

FIG. 6. Same as Fig. 3 but for 150 keV.

electron energy dependence of the doubly differential cross sections at small scattering angles (see Fig. 2). At projectile energies of 50 and 75 keV a clear shoulder structure is observed at the matching velocity. Again, this effect becomes weaker with increasing projectile velocity and no significant structure is seen at 150 keV. At 75 keV there appears to be an enhancement of the cross sections at electron velocities just below the matching velocity. This can be attributed to autoionization resonances for the $(2p^2)^1D$ and $(2s2p)^1P$ states. For a projectile energy of 75 keV, the resonance energies for these states correspond to a relative electron velocity close to one. The fact that we even find a structure at the matching velocity in the singly differential cross sections integrated over both the electron and the projectile angle shows that the effects of the PCI on the doubly differential cross sections are not merely due to a correlation between the projectile angle and the electron angle.

Our conclusion that the PCI significantly affects even the singly differential cross sections is also supported by our calculations. The $B1$ calculation, which does not include the PCI, does not show any structure at the matching velocity and it does not describe the shape of the experimental data well. The same calculation with the PCI included ($B2$), on the other hand, exhibits a very similar shoulder structure as the data at the matching velocity and describes the shape of the data fairly well. In the CTMC calculation, the effect does not appear to be as obvious probably due to the fewer calculated points. However, comparing the calculated points below the matching velocity to those above the matching velocity shows that there must be a change of slope somewhere around the matching velocity, at least for 50 keV.

While our $B2$ calculation is in good agreement with the

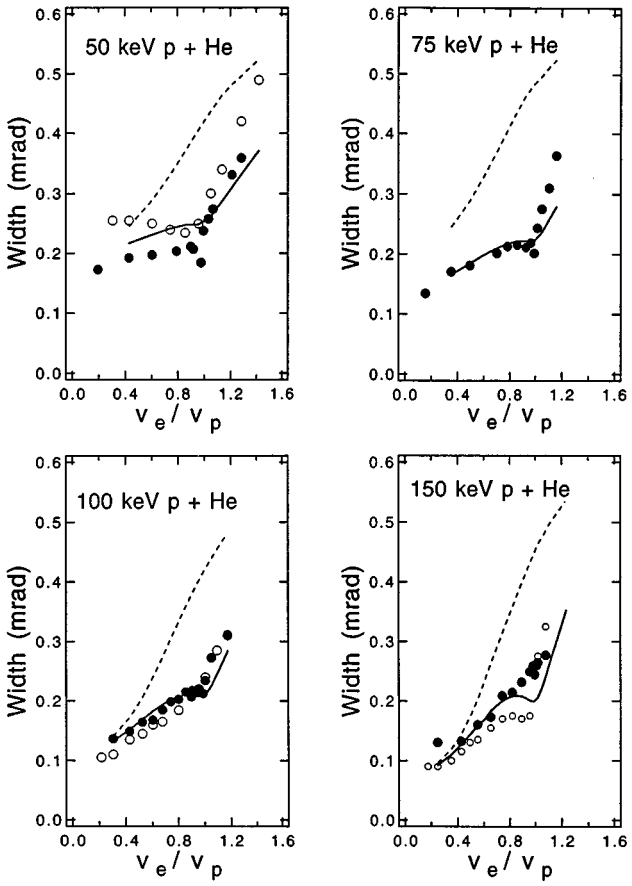

FIG. 7. Widths of the angular distributions of the doubly differential ionization cross sections as a function of the electron velocity relative to the projectile velocity. The curves and the open symbols represent the same calculations as in Fig. 3.

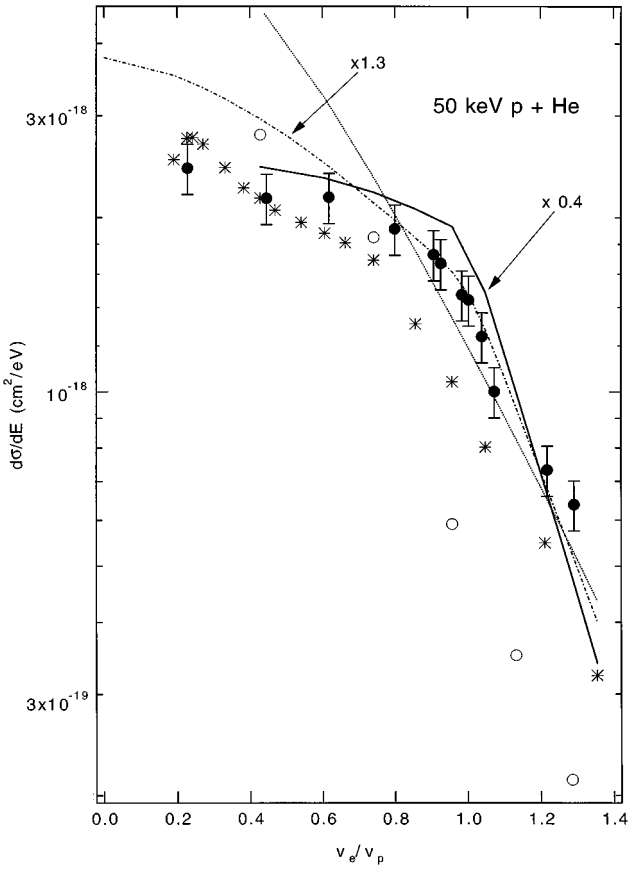

FIG. 8. Singly differential ionization cross sections as a function of the ionized electron velocity relative to the projectile velocity for 50-keV $p+$He collisions. The stars show experimental data of Cheng *et al.* [31] taken by electron spectroscopy. The dash-dotted curve is a CDW calculation by Gulyas *et al.* [36]. All the other symbols have the same meaning as in Fig. 3.

shape of the data, there are significant discrepancies in the magnitude especially for the low projectile energies. This is a result of the *ad hoc* method used to treat the PCI in this calculation. The PCI is accounted for by multiplying the scattering amplitudes by a Coulomb function, which has the form $1/(|v_e-v_p|)$. This will always increase the cross section near the velocity match and thus the total electron flux is not conserved in this calculation. On the other hand, the true effect of the PCI is just to redistribute the electron flux after the ionization process and thus it should not affect the total flux.

This total electron flux problem introduced by the PCI in our $B2$ calculation does not occur in the continuum distorted-wave (CDW) calculation by Gulyas *et al.* [36]. This calculation is very similar to the $B2$ calculation in that it also treats the target potential to all orders. However, the PCI is accounted for in a different way. In the CDW calculation, the PCI is incorporated *ab initio* in terms of a phase factor that the presence of the projectile potential after the collision introduces to the transition amplitude. Depending on the phase factor, the transition amplitude can now be either increased or decreased by the PCI and the total electron flux is not necessarily increased.

The CDW calculation is shown in Figs. 8–11 as the dash-dotted curves. Here, too, a shoulder structure at the matching velocity is apparent especially at the lower projectile energies. In the CDW calculation, the structure is not quite as pronounced as in the $B2$ calculation, but it is consistent with our data. A comparison in the magnitude of the CDW calculation, the experimental data and the two Born calculations also indicates that there does not appear to be the total electron flux problem encountered in the $B2$ calculation. The CDW calculation is in reasonable agreement with the magnitude in the data while the $B2$ calculation significantly overestimates the cross sections for small projectile energies. At the same time, the CDW and $B1$ calculations appear to yield similar cross sections integrated over the electron energy. Overall, the CDW calculation shows very good agreement with the data at small projectile energies. At higher projectile energies, increasing discrepancies in the shape are observed, while the agreement of the $B2$ calculation is improving.

It is also interesting to compare our measured singly differential cross sections to those obtained by electron spectroscopy. The stars in Figs. 8–11 show the electron data by Cheng *et al.* [31]. These data were not normalized to known total cross sections as were our data. The integrated cross sections of Cheng *et al.* are somewhat different but, within experimental uncertainties, not inconsistent with our integrated cross sections. Significant differences between our data and those of Cheng *et al.* are observed at the low projectile energies in the shape of the cross sections differential

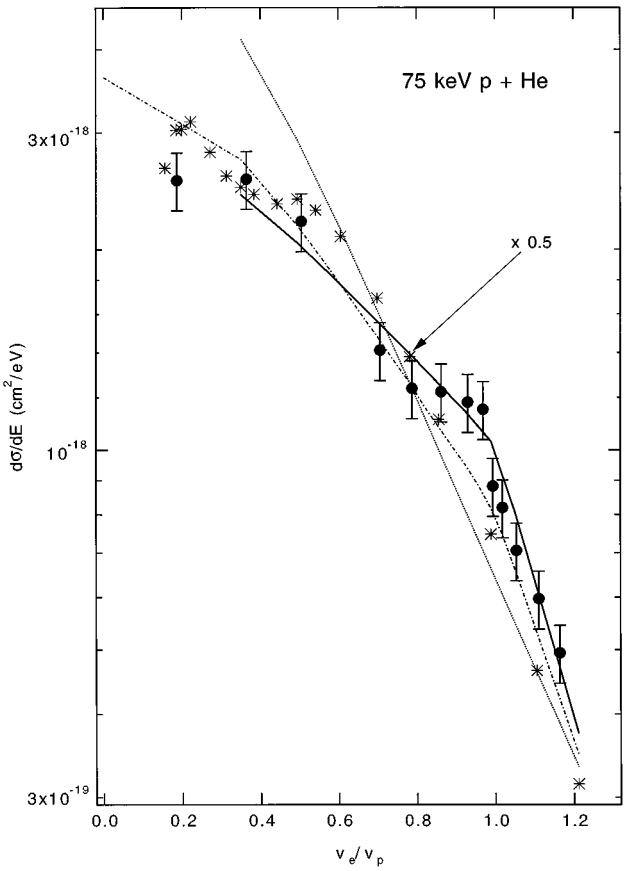

FIG. 9. Same as Fig. 8 but for 75 keV.

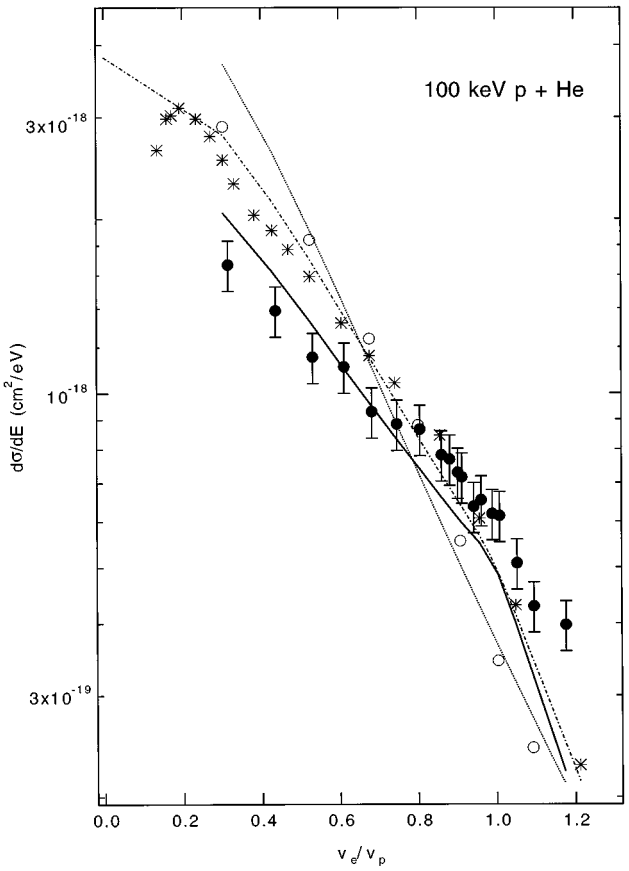

FIG. 10. Same as Fig. 8 but for 100 keV.

in the electron energy, however. Specifically, the electron data of Cheng *et al.* do not show any structure near the matching velocity; rather, the cross sections just fall off monotonically with increasing electron velocity. At 50 keV, however, there appears to be a structure at an electron velocity considerably below the matching velocity. These differences in the shape of the cross sections between our energy-loss data and the electron data can also be understood in terms of the PCI. In this context it is important to point out that the electron data were only taken for electron emission angles of 10° and larger. This means that most of the contributions from cusp electrons, which are mainly emitted in the forward direction, will not be seen. Our experiment, in contrast, automatically integrates over all electron angles. It is therefore not surprising that the effects of the PCI are more prominent in our data. At high projectile energies, where the influence of the PCI appears to be reduced, our data are in agreement with the electron data within experimental uncertainties.

The comparison of our measured singly differential cross sections to various calculations with and without the PCI as well as to the electron data, in which the PCI is suppressed, leads us to conclude that the PCI is very important even in the singly differential cross sections integrated over both the projectile scattering angle and the electron ejection angle, especially at small projectile energies. Gibson and Reid [37] have obtained an estimate for the total cusp electron production cross section for the same collision system and projectile energy regime as studied in this work. At 50 keV, for example, they obtained a value of about 2×10^{-18} cm^2. Along

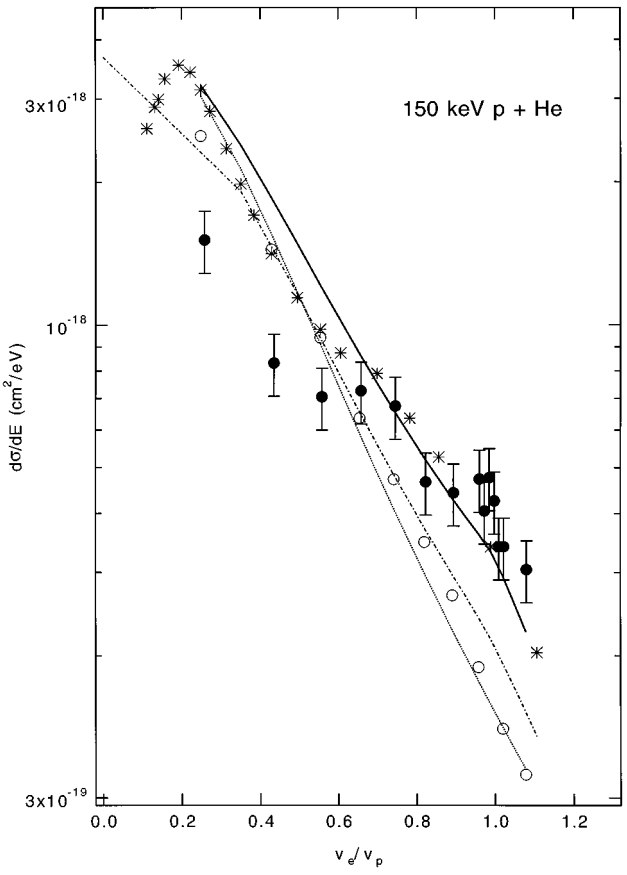

FIG. 11. Same as Fig. 8 but for 150 keV.

with the experimental width of the cusp peak (4 eV FWHM) in their work we crudely estimate the cross section differential in electron energy to be about 5×10^{-19} cm^2/eV at the cusp energy, which is about 20% of our measured differential ionization cross section. This value is consistent with the difference between our data and those of Cheng *et al.* Therefore, if one wants to determine singly differential ionization cross sections using electron spectroscopy, it is very important to take data at emission angles near 0°.

CONCLUSIONS

We have measured and calculated single ionization cross sections doubly differential in the projectile scattering angle and the ionized electron energy. We have for the first time observed the effects of the postcollision interaction on the heavy projectile spectra, both in the energy and in the angular dependence. By integrating over the projectile angle we also obtained singly differential cross sections as a function of the ionized electron energy. Our data show that the PCI significantly affects even the singly differential cross sections integrated over both the electron and the projectile angle, contrary to previous belief. A comparison with data obtained from electron spectroscopy shows that in electron measurements of singly differential cross sections it is critical to take data for electron angles around 0°.

It has been shown previously that, in theoretical calculations of single-ionization cross sections it is important to treat the target potential to all orders. Here, we demonstrated that the interaction between the projectile and ionized electron has to be treated beyond first order as well. Specifically, the long-range nature of the Coulomb force between the two free particles, leading to the PCI, can only be described in a higher-order treatment. In this context, our data provide a sensitive test case for the proper representation of the asymptotic three-body Coulomb wave function which is important for the description of the PCI. However, we also found that a classical treatment, which inherently includes the PCI, provides a good qualitative description of the ionization process.

ACKNOWLEDGMENTS

We would like to thank Dr. L. Gulyas, Dr. P. Fainstein, and Dr. A. Salin for making their calculations available to us prior to publication. This work was supported by the National Science Foundation, Grants No. PHY9020813 and No. PHY9116199 and by the Office of Fusion Energy, U.S. Department of Energy.

[1] J. T. Park, Adv. At. Mol. Phys. **19**, 67 (1983), and references therein.
[2] F. Martin and A. Salin, J. Phys. B **28**, 1985 (1995).
[3] J. F. Williams, J. Phys. B **14**, 1197 (1981).
[4] D. H. Madison, Comments At. Mol. Phys. **26**, 59 (1991).
[5] V. E. Bubelev, D. H. Madison, I. Bray, and A. T. Stelbovics, J. Phys. B **28**, 4619 (1995).
[6] M. Kimura and N. F. Lane, Adv. At. Mol. Phys. **26**, 79 (1990).
[7] B. H. Bransden and D. P. Dewangan, Adv. At. Mol. Phys. **25**, 343 (1989).
[8] J. H. McGuire, T. Reeves, N. C. Deb, and N. C. Sil, Nucl. Instrum. Methods B **24/25**, 243 (1987).
[9] S. Jones, D. H. Madison, A. Franz, and P. L. Altick, Phys. Rev. A **48**, 22 (1993).
[10] U. Fano, Phys. Rev. **124**, 1866 (1961).
[11] D. H. Madison, Phys. Rev. A **8**, 2449 (1973).
[12] G. B. Crooks and M. E. Rudd, Phys. Rev. Lett. **25**, 1599 (1970).
[13] K. G. Harrison and M. W. Lucas, Phys. Lett. **33A**, 142 (1970).
[14] J. Macek, Phys. Rev. A **1**, 235 (1970).
[15] A. Salin, J. Phys. B **2**, 631 (1969).
[16] W. Meckbach, I. B. Nemirovsky, and C. R. Garibotti, Phys. Rev. A **24**, 1793 (1981).
[17] W. Meckbach, P. J. Focke, A. R. Gõni, S. Suárez, J. Macek, and M. G. Menendez, Phys. Rev. Lett. **57**, 1587 (1986).
[18] G. C. Bernardi, S. Suárez, P. D. Fainstein, C. R. Garibotti, W. Meckbach, and P. Focke, Phys. Rev. A **40**, 6836 (1989).
[19] T. J. Gay, M. W. Gealy, and M. E. Rudd, J. Phys. B **23**, L823 (1990).
[20] W. Meckbach, S. Suárez, P. Focke, and G. Bernardi, J. Phys. B **24**, 3763 (1991).
[21] R. D. Dubois, Phys. Rev. A **48**, 1123 (1993).
[22] L. Sarkadi, J. Pálinkás, Á. Kövér, D. Berényi, and T. Vajnai, Phys. Rev. Lett. **62**, 527 (1989).
[23] S. Suárez, C. Garibotti, W. Meckbach, and G. Bernardi, Phys. Rev. Lett. **70**, 418 (1993).
[24] O. Jagutzki, R. Koch, A. Skutlarz, C. Kelbch, and H. Schmidt-Böcking, J. Phys. B **24**, 993 (1991).
[25] T. Vajnai, A. D. Gaus, J. A. Brand, W. Htwe, D. H. Madison, R. E. Olson, J. L. Peacher, and M. Schulz, Phys. Rev. Lett. **74**, 3588 (1995).
[26] R. Shakeshaft and L. Spruch, Phys. Rev. Lett. **41**, 1037 (1978).
[27] R. E. Olson, Phys. Rev. A **27**, 1871 (1983).
[28] R. E. Olson, T. J. Gay, H. G. Berry, E. B. Hale, and V. D. Irby, Phys. Rev. Lett. **59**, 36 (1987).
[29] C. O. Reinhold and R. E. Olson, Phys. Rev. A **39**, 3861 (1989).
[30] M. E. Rudd and D. H. Madison, Phys. Rev. A **14**, 128 (1976).
[31] W. Q. Cheng, M. E. Rudd, and Y. Y. Hsu, Phys. Rev. A **39**, 2359 (1989).
[32] A. D. Gaus, W. T. Htwe, J. A. Brand, T. J. Gay, and M. Schulz, Rev. Sci. Instrum. **65**, 3739 (1994).
[33] J. T. Park, J. M. George, J. L. Peacher, and J. E. Aldag, Phys. Rev. A **18**, 48 (1978).
[34] *Atomic Data for Fusion*, edited by C. F. Barnett (Oak Ridge National Laboratory, Oak Ridge, 1990).
[35] M. E. Rudd and D. H. Madison, Phys. Rev. A **14**, 128 (1976).
[36] L. Gulyas, P. D. Fainstein, and A. Salin, J. Phys. B **28**, 245 (1995).
[37] D. K. Gibson and I. D. Reid, J. Phys. B **19**, 3265 (1986).